

Enhanced hydrogen storage properties of Pd/Ti/Mg/Ti multilayer films using the catalytic effects of Pd

Hwaebong Jung, Sungmee Cho, and Wooyoung Lee

Citation: [Applied Physics Letters](#) **106**, 193902 (2015); doi: 10.1063/1.4921274

View online: <http://dx.doi.org/10.1063/1.4921274>

View Table of Contents: <http://scitation.aip.org/content/aip/journal/apl/106/19?ver=pdfcov>

Published by the [AIP Publishing](#)

Articles you may be interested in

[Divacancies and the hydrogenation of Mg-Ti films with short range chemical order](#)

Appl. Phys. Lett. **96**, 121902 (2010); 10.1063/1.3368698

[Hydrogenation of Mg film and Mg nanoblade array on Ti coated Si substrates](#)

Appl. Phys. Lett. **93**, 163114 (2008); 10.1063/1.3003880

[Hydrogen absorption kinetics and optical properties of Pd-doped Mg thin films](#)

J. Appl. Phys. **100**, 023515 (2006); 10.1063/1.2214208

[Comparative study of polycrystalline Ti, amorphous Ti, and multiamorphous Ti as a barrier film for Cu interconnect](#)

J. Vac. Sci. Technol. B **23**, 229 (2005); 10.1116/1.1852466

[Temperature and doping-dependent resistivity of Ti/Au/Pd/Au multilayer ohmic contact to n-GaN](#)

J. Appl. Phys. **91**, 9218 (2002); 10.1063/1.1471390



MMR TECHNOLOGIES

**THE WORLD'S RESOURCE FOR
VARIABLE TEMPERATURE
SOLID STATE CHARACTERIZATION**

WWW.MMR-TECH.COM

OPTICAL STUDIES SYSTEMS SEEBECK STUDIES SYSTEMS MICROPROBE STATIONS HALL EFFECT STUDY SYSTEMS AND MAGNETS

Enhanced hydrogen storage properties of Pd/Ti/Mg/Ti multilayer films using the catalytic effects of Pd

Hwaebong Jung, Sungmee Cho,^{a)} and Wooyoung Lee^{a)}

Department of Materials Science and Engineering, Yonsei University, 262 Seongsanno Seodaemun-gu, Seoul 129-749, South Korea

(Received 26 March 2015; accepted 6 May 2015; published online 14 May 2015)

Here, we report the microstructural and hydrogen storage properties of a 40-layer film of Pd (x nm)/Ti (40 nm)/Mg (360 nm)/Ti (40 nm) (x = 0, 5, 10, and 20) fabricated using an ultra-high vacuum DC magnetron sputtering system. The superior hydrogen uptake of the Pd/Ti/Mg/Ti films was 6.42 wt. % for x = 10 at 150 °C. The hydrogen absorption time is strongly dependent on the Pd film thickness (0–40 nm). As a result, the Pd/Ti/Mg/Ti multilayer film with the Pd interlayer can be attributed to offer the further diffusion channels and the controlled growth rate of hydride formation at the Pd/Ti/Mg interfaces, which provides an overall enhancement of the hydrogen storage properties. © 2015 AIP Publishing LLC. [<http://dx.doi.org/10.1063/1.4921274>]

Hydrogen has been suggested as a prospective alternative to carbon-based fuels for future clean energy systems. Among hydrogen storage materials, magnesium (Mg) is considered to be a great potential material because of its benefits of high volumetric ($\sim 110 \text{ kgH}_2/\text{m}^3$)/gravimetric (7.6 wt. %, MgH_2) hydrogen storage capacity, low cost, accessibility, and reversibility. On the other hand, Mg-based materials have several problems to overcome before they can be used for commercial applications, such as slow MgH_2 reaction kinetics due to the poor catalytic activity of the Mg surface toward hydrogen dissociation and the low hydrogen diffusivity of MgH_2 .¹ Many studies have attempted to improve the reaction kinetics of Mg through size control and through the modification of hydrogenation temperatures using a ball milling process,^{2,3} additives,^{4,5} catalysts,^{6–9} polymer layers,¹⁰ and thin films.^{11–33} In particular, Mg-based thin films with transition metal catalysts have been demonstrated to be effective for enhancing the performance of magnesium hydrides. For example, studies on Mg/Pd films showed that Pd not only prevents the oxidation of Mg but also acts as a good catalyst for the dissociation/recombination of hydrogen.^{11–17} However, poor hydrogenation kinetics was observed since binary intermetallic Mg–Pd alloys were formed at 373 K.^{14,17} Previously, Mg-based bilayer films such as MgAl,²² MgNi,²³ MgTi,^{25,26} MgV,²⁷ and MgCr²⁷ have been shown to have enhanced H_2 absorption behavior, which resulted in rapid kinetics at low temperatures. Among these, Ti in Mg/Ti multilayered structures widely used to control of strain and interface energy and to prevent inter-diffusion between Mg and Pd.^{26,34,35} Moreover, Mg-based multilayer films, including Mg/Al/Ti,²⁸ Mg/Fe/Ti,²⁹ and Pd/Ti/Mg/Ti,³⁰ have also reported and shown superior absorption/desorption hydrogen kinetics at relatively reduced temperatures. However, multilayer films as a function of Pd layer thickness have not been studied for hydrogen storage applications.

In this work, we report the Pd catalytic effects on the microstructural evolution and hydrogen storage properties of

Pd/Ti/Mg/Ti multilayer films at various thicknesses of the Pd film interlayer. Based on our previous study,³⁰ the insertion of Ti interlayers between Mg and Pd prevents inter-diffusion at the Mg/Pd interface and improves the absorption behavior of Mg during hydrogenation. In this regard, the Pd/Ti/Mg/Ti multilayer film with various thicknesses of the Pd interlayers can allow additional diffusion paths for the hydrogen atoms through an additional interface for hydrogenation and can control the growth rate of hydride formation at the interface, which enhances the kinetics and capacity in Pd/Ti/Mg/Ti multilayer films under a hydrogen pressure of 30 bars at diverse temperatures.

Forty multilayers of Pd (x nm)/Ti (40 nm)/Mg (360 nm)/Ti (40 nm) films (x = 0, 5, 10, and 20) were deposited on a glass substrate (25 × 75 mm), and the top Ti surface was capped with a Pd (40 nm) layer via ultra-high vacuum DC magnetron sputtering in an Ar atmosphere. The deposition process was performed below 5.0×10^{-3} Torr for Mg and below 2.5×10^{-3} Torr for both Pd and Ti in Ar at a flow rate of 34 sccm with a base pressure of 4×10^{-8} Torr. The typical deposition rates of multilayer films at room temperature were $\sim 12.9 \text{ \AA/s}$ for Mg at 50 W, $\sim 1.7 \text{ \AA/s}$ for Ti at 50 W, and $\sim 4 \text{ \AA/s}$ for Pd at 20 W. The purity of the Mg, Ti, and Pd targets was 4N. Microstructural characteristics were evaluated using X-ray diffraction (XRD, Ultima IV/ME 200DX, Rigaku) and cross-sectional transmission electron microscopy (TEM, JEOL JEM ARM 200F) with energy dispersive X-ray (EDX, X Max Oxford). Prior to cross-sectional TEM observation, the samples were cut perpendicular to the surface using a focused ion beam system (FIB, JEOL JIB 4601F). The hydrogen uptake was measured using a magnetic suspension microbalance (Rubotherm, Isosorp) via a gravimetric method performed under a hydrogen pressure of 30 bars or vacuum in the temperature ranges of 50–150 °C. The amount of sample used for the measurements was about 0.1–0.2 g. All sorption isotherms were obtained using ultra-high purity gases (H_2 : 99.999%; He: 99.99%).³⁰

Fig. 1 shows a schematic illustration of the hydrogenation process in the 40 multilayers of Pd/Ti/Mg/Ti films (a)

^{a)}Electronic addresses: wooyoung@yonsei.ac.kr and csmise@yonsei.ac.kr

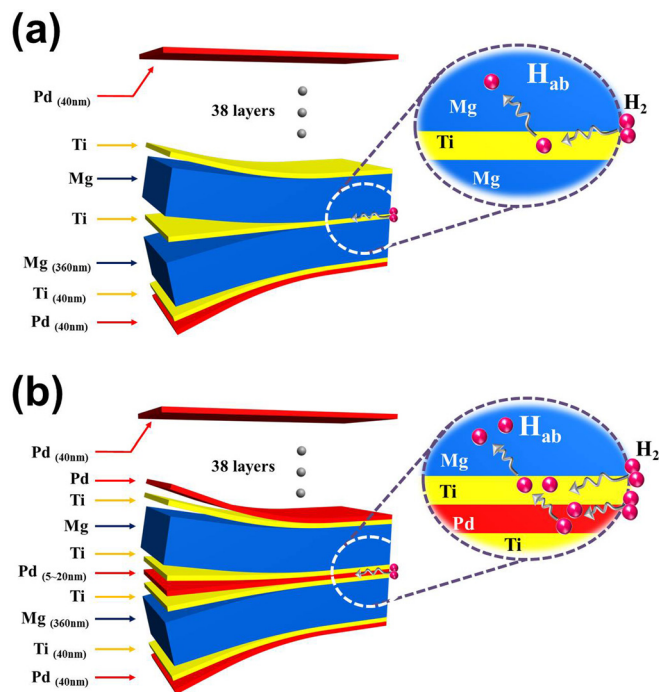


FIG. 1. Schematic illustrations of the hydrogenation process in the 40 multi-layers of Pd/Ti/Mg/Ti films (a) without and (b) with Pd film ranging from 5 to 20 nm.

without and (b) with Pd film in the range of 5–20 nm. In Pd/Ti/Mg/Ti multilayer films without the Pd film, hydrogen dissociation only occurs on exposed Ti catalyst surface, while a small amount of MgH_2 hydride nucleates at the Ti/Mg interface. However, Pd/Ti/Mg/Ti multilayer films with the Pd films adsorb a relatively large amount of H_2 molecules though both the Ti and Pd catalyst surfaces, e.g., absorbed hydrogen atoms at Pd layers diffuse into the Ti layers to form titanium hydride and hydrogen atoms simultaneously are sucked into the Ti layer. This is thermodynamically due to Ti (-130 kJ/mol H_2) has a lower enthalpy than of the hydride formation Pd (-38 kJ/mol H_2). The Mg layers start to absorb hydrogen atoms through Ti/Mg interfaces after all Ti layers have been hydrogenated for MgH_2 formation. In other words, additional diffusion paths through the Ti/Pd surface layers could allow a significant amount of hydrogen atoms to diffuse into the Mg metal layer for H_2 dissociation, and the Pd interlayer, which is a promising catalyst, can be used to control the growth rate for hydride formation at an interface. Finally, further hydrogenation can be affected by changes in the distribution of the Pd catalyst.

The hydrogenation properties of the Pd/Ti/Mg/Ti multilayer films without and with the Pd films (5–40 nm) were measured under 30 bars of hydrogen at 150°C for 10 h, as shown in Figure 2. The hydrogen absorption capacity for the Pd/Ti/Mg/Ti film was 2.44, 3.87, 6.42, 5.35, and 4.35 wt. % for $x = 0, 5, 10, 20,$ and 40 , respectively, as shown in Figure 2(a). For comparison with our previous data,³⁶ the data for $x = 40$ were included in the plots. The best absorption progress in the Pd/Ti/Mg/Ti multilayer films occurs when the Pd film is 10-nm thick, and the hydrogen absorption capacities decrease with increasing the Pd film thickness due to the low theoretical hydrogen storage capacity of Pd. However, the

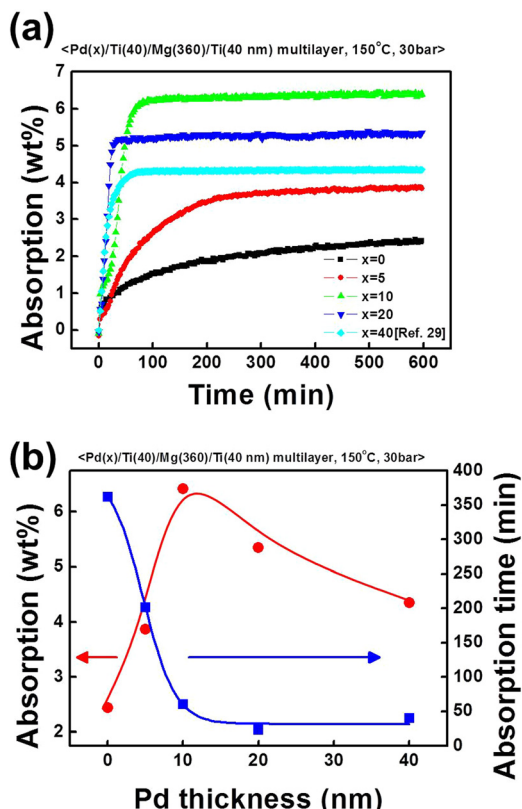


FIG. 2. Hydrogenation properties of Pd/Ti/Mg/Ti multilayer films without and with Pd film (5–40 nm) under 30 bars of hydrogen at 150°C for 10 h. (a) Hydrogen absorption capacities vs. time and (b) hydrogen absorption capacities (red arrow) and absorption time (blue arrow) vs. different Pd film thicknesses.

hydrogen absorption time as shown in Fig. 2(b), the Pd/Ti/Mg/Ti multilayer film without the Pd film shows remarkably slow kinetics, whereas the multilayer films with the Pd interlayers revealed the decreased hydrogen absorption time. It is assumed that Mg covered with both Ti and Pd induces faster kinetics than Mg covered with Ti, i.e., in the Ti/Mg structures, MgH_2 formation occurs from Ti to Mg ($\Delta H_{\text{Mg}} = -74.4 \text{ kJ/mol H}_2 > \Delta H_{\text{Ti}} = -130 \text{ kJ/mol H}_2$). However, addition of Pd as catalyst supports further diffusion of hydrogen atoms into Ti ($\Delta H_{\text{Pd}} = -38 \text{ kJ/mol H}_2 > \Delta H_{\text{Ti}} = -130 \text{ kJ/mol H}_2$) in the Pd/Ti/Mg structures, which leads to an increase of Mg hydride growth rate with saturated hydrogenation ($\Delta H_{\text{Ti}} < \Delta H_{\text{Mg}} < \Delta H_{\text{Pd}} < 0$).³⁷ An overview of the data shows that the hydrogen absorption time decreased to until 10-nm-thick Pd film and then the absorbed hydrogen fully saturated at absorption time of 23–60 min in the thickness range 10–40 nm, from 362 min for $x = 0$ to 201 min for $x = 5$, to 60 min for $x = 10$, to 23 min for $x = 20$, and to 39 min for $x = 40$. Based on these results, the various thicknesses of the Pd layers in the multilayer structures showed that diffusion of hydrogen atoms through the growing hydride layer determines the rate of the hydride formation, indicating that additional interface energy by employing Pd layers help to reduce the energy barrier for Mg hydride formation occurs mostly at the Pd/Ti/Mg interfaces.

The hydrogen absorption capacities were tested as a function of temperature in the 50 – 150°C range for 10 h under 30 bars of hydrogen, as shown in Fig. 3(a). The

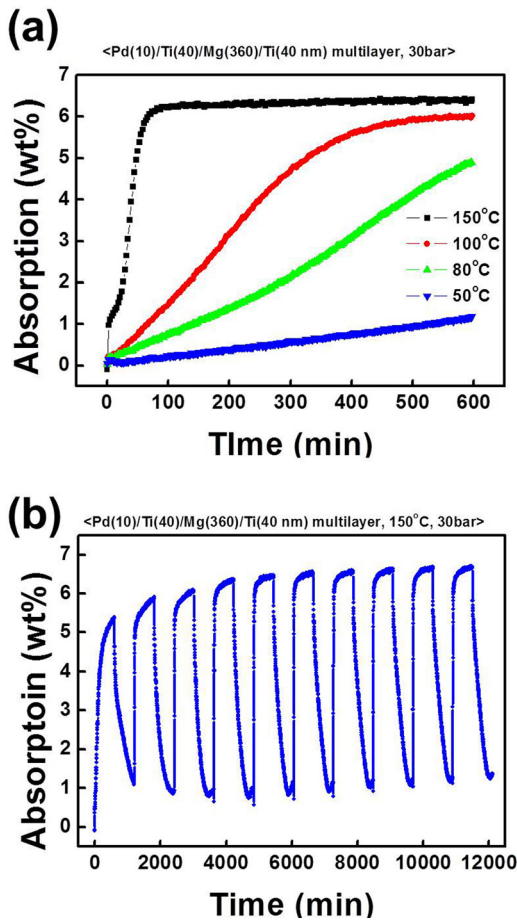


FIG. 3. (a) Hydrogen absorption capacities as a function of temperature in the range from 50 to 150 °C for 10 h under 30 bars of hydrogen, and (b) a cycling test on the best performing multilayer film with a 10-nm Pd interlayer up to 10 cycles.

hydrogen absorption capacities for the Pd/Ti/Mg/Ti multilayer films increase with increasing temperature, showing a fast growth rate of the MgH_2 hydride. Generally, the absorbed hydrogen weight percent and hydrogenation rate increase with increasing hydrogen storage temperature. At lower temperatures, the rate of hydrogen absorption was decreased due to the lack of the activation energy for the MgH_2 hydride formation. To assess the absorption/desorption behavior of the Pd/Ti/Mg/Ti multilayer film, a cycling test was conducted on the best performing multilayer film, which had a 10-nm-thick Pd layer, under 30 bars of hydrogen/vacuum at 150 °C for 10 h up to 10 cycles, as shown in Fig. 3(b). The first few cycles show relatively slow kinetics; however, the absorption/desorption behavior starts to reach a stable stage after four cycles and saturated at 6.67 wt. %.

Fig. 4 shows the XRD patterns of (a) the Pd/Ti/Mg/Ti multilayer films without and with the Pd films (5–20 nm) after dehydrogenation under vacuum at 150 °C and (b) the best performing multilayer films with a 10-nm-thick Pd interlayer after dehydrogenation under vacuum in the temperature range of 50–100 °C. All detected patterns indicated that Mg (JCPDS: #35–0821) and Ti (JCPDS: #44–1294) formed hexagonal phases. On the other hand, Pd (JCPDS: #46–1043) formed a cubic phase without forming secondary phases such as Mg_xPd_y intermetallic compounds in any of the Pd film thicknesses, as shown in Fig. 4(a). The growth of the Mg film shows that the (002) and (004) orientations are preferred, while the overlapping sharp peaks correspond to the Pd (111) and Ti (101) orientations. The intensity variations of the Pd (111) peak reveal an increase in the Pd film thickness. Fig. 4(b) also confirms the Mg, Ti, and Pd phases with no interdiffusion of Mg–Pd alloys in the Pd/Ti/Mg/Ti films after dehydrogenation at 50, 80, and 100 °C.

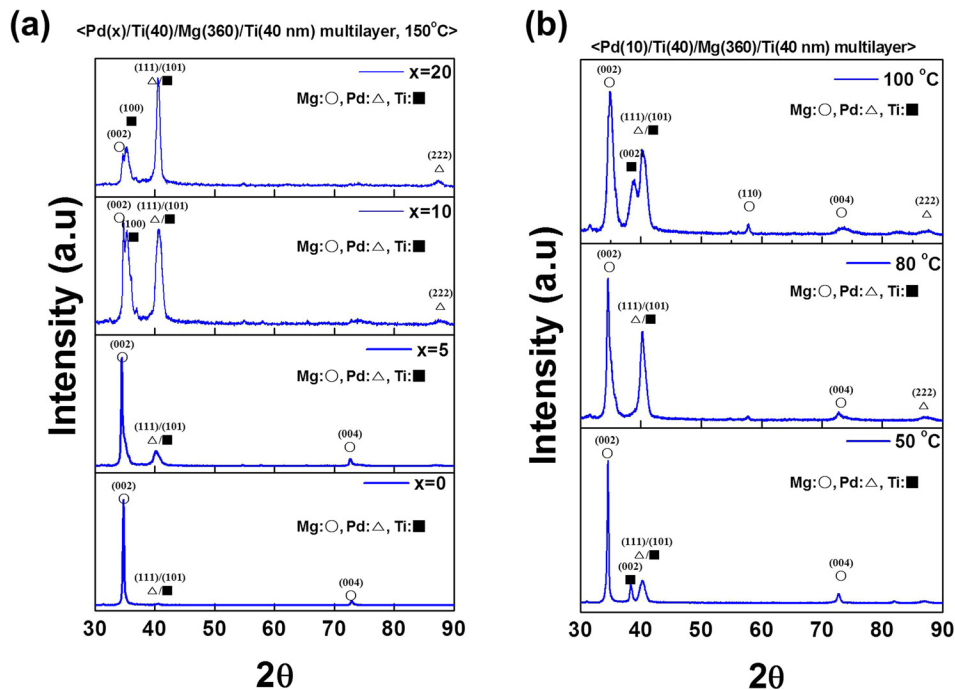


FIG. 4. The XRD patterns of (a) Pd/Ti/Mg/Ti multilayer films without and with Pd film (5–20 nm) after dehydrogenation under vacuum at 150 °C and (b) the best performing multilayer films with a 10-nm Pd film after dehydrogenation under vacuum in the temperature range from 50 to 100 °C.

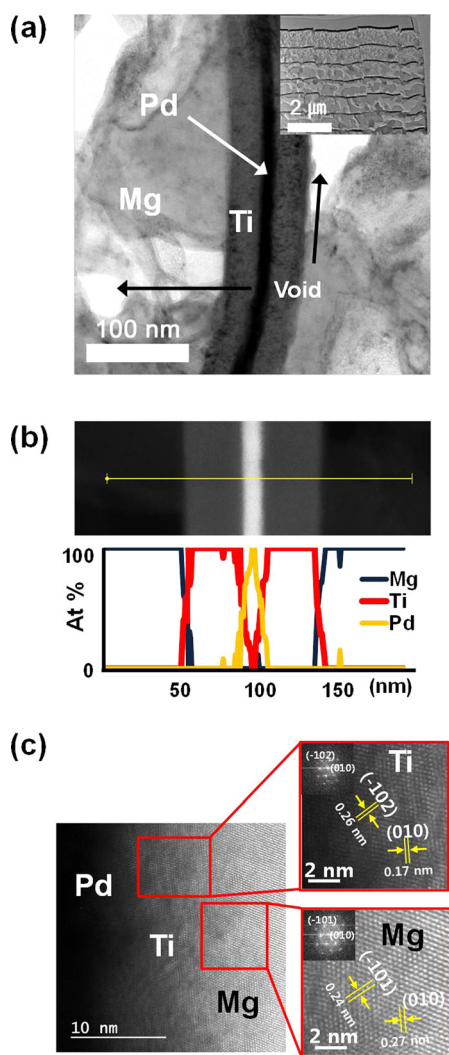


FIG. 5. (a) Cross-sectional TEM images, (b) EDX line profile of the multilayered Pd (10 nm)/Ti (40 nm)/Mg (360 nm)/Ti (40 nm) films under 30 bars of hydrogen/vacuum at 150 °C for 10 h after 10 cycles, and (c) cross-sectional HRTEM image of the Pd (40 nm)/Ti (10 nm)/Mg (360 nm)/Ti (40 nm) multilayer after hydrogenation/dehydrogenation. The insets show the selected area diffraction (SAD) patterns of the Mg and Ti layers.

Fig. 5 shows cross-sectional TEM images with the EDX line profile of multilayered Pd (10 nm)/Ti (40 nm)/Mg (360 nm)/Ti (40 nm) films under 30 bars of hydrogen/vacuum at 150 °C for 10 h after 10 cycles. The low-resolution image in the inset of Fig. 5(a) shows a stack of several Mg, Ti, and Pd layers, while the high-resolution image shows a clear deformation of the porous structure in the Mg layer, exhibiting a large volume expansion of the Mg layer due to the incorporated voids.³² In particular, the thickness of the Mg layer was extended to 670 nm. Such volume expansion starts to occur during the hydrogenation/dehydrogenation of Mg, and then potential nucleation sites in both the hydride and metal phase move apart. Thus, Mg layer begins to grow thicker due to aggregation of Mg during repeated cycles.³⁸ The EDX scan profile in Fig. 5(b) confirms the clear interface between individual layers with an absence of the Mg–Pd compound after cycling, which agrees with the XRD data. The film thicknesses of both Ti and Pd catalyst layers were not changed since Ti is non-reactive material with Mg, showing film thicknesses of

10 nm for Pd and 40 nm for Ti after cycling. Fig. 5(c) shows a cross-sectional high-resolution TEM (HRTEM) image of dehydrogenated Pd (40 nm)/Ti (10 nm)/Mg (360 nm)/Ti (10 nm) multilayer film. As shown in the TEM images, a stack of Mg, Ti, and Pd layers can be clearly observed based on their contrast difference, e.g., higher atomic number material appears brighter than low atomic number material. Both Mg and Ti layers are well crystallized and are composed of hexagonal crystals with preferred orientations of (010)_{Mg} and (010)_{Ti} in the corresponding selected area diffraction patterns (SEAD) in the insets. The measured d-spacing values of (010) and (−101) planes for Mg are 0.27 nm and 0.24 nm, respectively, and d-spacings of (010) and (−102) planes of Ti was measured 0.17 nm and 0.26 nm, respectively. Hexagonal structures of Mg and Ti with the calculated lattice parameters ($a = 0.32$ nm, $c = 0.52$ nm for Mg, $a = 0.30$ nm, and $c = 0.67$ nm for Ti) are a good match with previous report.³⁹

In summary, we investigated microstructural evolution and hydrogen storage properties of Pd/Ti/Mg/Ti multilayer films using further catalytic effects of Pd. The addition of the Pd layers in Pd (x nm)/Ti (40 nm)/Mg (360 nm)/Ti (40 nm) multilayer films could significantly enhance the hydrogen absorption kinetics. The XRD and EDX line scan profile analyses confirmed the absence of Mg–Pd intermetallic phases in the Pd/Ti/Mg/Ti film after cycling tests, and the TEM images showed that the Mg film expanded by a certain volume ratio with the formation of voids during repeated cycles. We conclude that the measured hydrogenation properties of the Pd/Ti/Mg/Ti films with the inserted Pd films showed a dramatic enhancement, indicating provision of the large amount of diffusion channels for hydrogen atoms and control of the growth rate for the hydride formation at the Pd/Ti/Mg interfaces.

This work was supported by the Priority Research Centers Program (2009-0093823) and POSCO Research Project through the National Research Foundation of Korea (NRF).

- ¹A. M. Seayad and D. M. Antonelli, *Adv. Mater.* **16**, 765 (2004).
- ²L. Zaluski, A. Zaluska, and J. O. Ström-Olsen, *J. Alloys Compd.* **217**, 245 (1995).
- ³A. Zaluska, L. Zaluski, and J. O. Ström-Olsen, *J. Alloys Compd.* **289**, 197 (1999).
- ⁴N. Bazzanella, R. Checchetto, and A. Miotello, *Appl. Phys. Lett.* **92**, 051910 (2008).
- ⁵S. Orimo, K. Ikeda, H. Fujii, Y. Fujikawa, Y. Kitano, and K. Yamamoto, *Acta Mater.* **45**, 2271 (1997).
- ⁶N. Hanada, T. Ichikawa, and H. Fujii, *J. Phys. Chem. B* **109**, 7188 (2005).
- ⁷M. Dornheim, S. Doppiu, G. Barkhordarian, U. Boesenberg, T. Klassen, O. Gutfleisch, and R. Bormann, *Scr. Mater.* **56**, 841 (2007).
- ⁸L. Xie, Y. Liu, Y. T. Wang, J. Zheng, and X. G. Li, *Acta Mater.* **55**, 4585 (2007).
- ⁹M. Polanski and J. Bystrzycki, *J. Alloys Compd.* **486**, 697 (2009).
- ¹⁰K. Jeon, H. R. Moon, A. M. Ruminiski, B. Jiang, C. Kisielowski, R. Bardhan, and J. J. Urban, *Nat. Mater.* **10**, 286 (2011).
- ¹¹G. L. N. Reddy, S. Kumar, Y. Sunitha, S. Kalavathi, and V. S. Raju, *J. Alloys Compd.* **481**, 714 (2009).
- ¹²S. Barcelo, M. Rogers, C. P. Grigoropoulos, and S. S. Mao, *Int. J. Hydrogen Energy* **35**, 7232 (2010).
- ¹³S. Singh, S. W. H. Eijt, M. W. Zandbergen, W. J. Legerstee, and V. L. Svetchnikov, *J. Alloys Compd.* **441**, 344 (2007).
- ¹⁴K. Higuchi, H. Kajioka, K. Toiyama, H. Fujii, S. Orimo, and Y. Kikuchi, *J. Alloys Compd.* **293**, 484 (1999).

- ¹⁵K. Higuchi, K. Yamamoto, H. Kajiooka, K. Toiyama, M. Honda, S. Orimo, and H. Fujii, *J. Alloys Compd.* **330**, 526 (2002).
- ¹⁶S. Y. Ye, S. L. I. Chan, L. Z. Ouyang, and M. Zhu, *J. Alloys Compd.* **504**, 493 (2010).
- ¹⁷S. Bouhitiyya and L. Roué, *Int. J. Hydrogen Energy* **34**, 5778 (2009).
- ¹⁸T. J. Richardson, J. L. Slack, R. D. Armitage, R. Kostecki, B. Farangis, and M. D. Rubin, *Appl. Phys. Lett.* **78**, 3047 (2001).
- ¹⁹A. Borgschulte, R. J. Westerwaal, J. H. Rector, B. Dam, R. Griessen, and J. Schoenes, *Phys. Rev. B* **70**, 155414 (2004).
- ²⁰A. Borgschulte, R. Gremaud, S. de Man, R. J. Westerwaal, J. H. Rector, B. Dam, and R. Griessen, *Appl. Surf. Sci.* **253**, 1417 (2006).
- ²¹D. M. Borsa, A. Baldi, M. Pasturel, H. Schreuders, B. Dam, R. Griessen, P. Vermeulen, and P. H. L. Notten, *Appl. Phys. Lett.* **88**, 241910 (2006).
- ²²G. Garcia, R. Doménech-Ferrer, F. Pi, J. Santiso, and J. Rodríguez-Viejo, *J. Comb. Chem.* **9**, 230 (2007).
- ²³M. Pasturel, R. J. Wijngaarden, W. Lohstroh, H. Schreuders, M. Slaman, B. Dam, and R. Griessen, *Chem. Mater.* **19**, 624 (2007).
- ²⁴X. Tan, C. T. Harrower, B. S. Amirkhiz, and D. Mitlin, *Int. J. Hydrogen Energy* **34**, 7741 (2009).
- ²⁵G. Xin, J. Yang, H. Fu, W. Li, J. Zheng, and X. Li, *RSC Adv.* **3**, 4167 (2013).
- ²⁶A. Baldi, G. K. Pálsson, M. Gonzalez-Silveira, H. Schreuders, M. Slaman, J. H. Rector, G. Krishnan, B. J. Kooi, G. S. Walker, M. W. Fay, B. Hjörvarsson, R. J. Wijngaarden, B. Dam, and R. Griessen, *Phys. Rev. B* **81**, 224203 (2010).
- ²⁷C. M. P. Fry, D. M. Grant, and G. S. Walker, *Int. J. Hydrogen Energy* **39**, 1173 (2014).
- ²⁸R. Zahiri, B. Zahiri, A. Kubis, P. Kalisvaart, B. S. Amirkhiz, and D. Mitlin, *Int. J. Hydrogen Energy* **37**, 4215 (2012).
- ²⁹B. Zahiri, C. T. Harrower, B. S. Amirkhiz, and D. Mitlin, *Appl. Phys. Lett.* **95**, 103114 (2009).
- ³⁰H. Jung, J. Yuh, S. Cho, and W. Lee, *J. Alloys Compd.* **601**, 63 (2014).
- ³¹L. Z. Ouyang, H. Wang, M. Zhu, J. Zou, and C. Y. Chung, *Microsc. Res. Tech.* **64**, 323 (2004).
- ³²L. Z. Ouyang, S. Y. Ye, H. W. Dong, and M. Zhu, *Appl. Phys. Lett.* **90**, 021917 (2007).
- ³³M. K. Dietrich, A. Laufer, G. Haas, A. Polity, and B. K. Meyer, *Sens. Actuators, A* **206**, 127 (2014).
- ³⁴A. Baldi, M. Gonzalez-Silveira, V. Palmisano, B. Dam, and R. Griessen, *Phys. Rev. Lett.* **102**, 226102 (2009).
- ³⁵L. P. A. Mooij, A. Baldi, C. Boelsma, K. Shen, M. Wagemaker, Y. Pivak, H. Schreuders, R. Griessen, and B. Dam, *Adv. Energy Mater.* **1**, 754 (2011).
- ³⁶H. Jung, S. Cho, and W. Lee, *J. Alloys Compd.* **635**, 203 (2015).
- ³⁷A. Baldi, V. Palmisano, M. Gonzalez-Silveira, Y. Pivak, M. Slaman, H. Schreuders, B. Dam, and R. Griessen, *Appl. Phys. Lett.* **95**, 071903 (2009).
- ³⁸W. P. Kalisvaart, A. Kubis, M. Danaie, B. S. Amirkhiz, and D. Mitlin, *Acta Mater.* **59**, 2083 (2011).
- ³⁹Y. Wang, S. Curtarolo, C. Jiang, R. Arroyave, T. Wang, G. Ceder, L.-Q. Chen, and Z.-K. Liu, *Comput. Coupling Phase Diagrams Thermochem.* **28**, 79 (2004).